Supporting information

Host-guest compound formed by $Cu_3[P_2W_{18}O_{62}]$ and HKUST-1 with capacitance and H_2O_2 sensing properties

Caihong Shi, Shan Di, Hongquan Jiang*, Chunxiao Wang, Chunmei Wang, Kai Yu*, Jinghua Lv, Baibin Zhou*

Key Laboratory for Photonic and Electronic Bandgap Materials, Ministry of Education, Harbin Normal University, Harbin 150025, P. R. China.
*Corresponding authors.
E-mail addresses: h.q.jiang1119@163.com; hlyukai188@163.com; zhou_bai_bin@163.co

Contents

1. Experimental Section

1.1 Synthesis method

1.1.1 Synthesis of $Cu_3[P_2W_{18}O_{62}]$

$K_6P_2W_{18}O_{62}\cdot 15H_2O$ (0.3 mmol) and $Cu(NO_3)_2\cdot 6H_2O$ (0.9 mmol) were added to 10 mL distilled water and dissolved at room temperature. After stirring with magnetic stirrer for 5 h, the turbid liquid was centrifuged and washed with absolute ethanol three times and drying at 60 ℃ for 24 h. A light green powder was obtained.

1.1.2 Synthesis of HKUST-1

H_3BTC (0.667 mmol), $Cu(NO_3)_2\cdot 6H_2O$ (1.005 mmol) were mixed in an agate mortar with a little of ethanol and ground with 3~5 kg force for 2 h. The product was centrifuged and washed with ethanol three times and dried to obtain blue sample at 60 ℃.

1.1.3 Synthesis of physical mixtures

$Cu_3[P_2W_{18}O_{62}]$ (0.5 mmol) and HKUST-1 (1 mmol) were mixed evenly according to the ratio of $Cu_3[P_2W_{18}O_{62}]$@HKUST-1 to get the physical mixture of blue-green.

1.2 Test methods

1.2.1 Experimental instruments

Infrared spectrometer: Brucker, VER TEX 80, Germany. X-ray powder diffractometer: Brucker, D8ADVANCE, Germany. Aultrahigh resolution scanning electron microscope: JEOL, JSM-7600F, Japan. Transmission electron microscope: FEI, Tecnai F20, America. Specific surface area analyzer: Micromeritics, ASAP 2460, America. X-ray source electron spectrometer: Kratos, AXIS ULTRA DLD, UK. Thermogravimetric analyzer: Perkin Elmer, Diamond 6300, America. Inductively Coupled Plasma Mass Spectrometer: Perkin Elmer, NexION 300X, America. Electrochemical workstation: Chenhua ShangHai, CHI660E, China. Constant temperature magnetic agitator: Guohuang Changzhou, HJ-3, China. Table centrifuge: Anting Shanghai, KA-1000, China. Electronic analytical balance: Setori Beijing, BS124S, China. Electric heating constant temperature blast drying oven: Yiheng Shanghai, DHG-9075A, China.

1.2.2 Characterization Measurements

All reagents were purchased and used without further purification. Human serum samples were purchased from Beijing Solaibao Technology Co., LTD. Fourier transform infrared spectroscopy (FT-IR) was carried out with KBr pellets containing the samples. Powder X-ray diffraction (XRD) using Cu Kα radiation (λ = 0.154 nm) was employed to identify the crystalline phase of the material and the range of 2θ from 5-90°. The scanning electron microscopy (SEM) images were collected by aultrahigh resolution scanning electron microscope and the transmission electron microscope (TEM) are collected by transmission electron microscope which can observe the morphology. The Brunauer-Emmett-Teller (BET) surface area was collected by N_2 adsorption measurements at 77.3 K (Nova 2000E). X-ray photoelectron spectroscopy (XPS) analyses were carried out using a Mg Kα (1253.6 eV) achromatic X-ray source electron spectrometer. The thermogravimetric (TG) analyzer manufactured was used to test the change of sample weight with temperature or time. The ICP analyzer was performed in ICP-MS: Perkin Elmer, NexION 300X analyzer.

1.2.2 Electrochemical measurements for supercapacitors

All electrochemical measurements were conducted on an electrochemical workstation (CHI660E, Chenhua ShangHai, China). A three-electrode system was used to investigate the electrochemical performances of the individual electrodes. A platinum foil (1×1 cm^{-2}) and Ag/AgCl were used as the counter electrode and the reference electrodes, respectively. Cyclic voltammetry (CV) and galvanostatic charge/discharge (GCD) were tested with -0.4-0.6 V and the electrochemical impedance (EIS) was performed with the frequency range from 0.01 Hz to 100 kHz. Then CV, GCD and EIS also were used to appraise the electrochemical performance of supercapacitors in the two-electrode system.

1.2.3 Electrochemical measurements for sensors

Glassy carbon electrode (GCE) was used as working electrode, Ag/AgCl as reference electrode and Pt as counter electrode. The H_2O_2 sensing performance was performed in 0.1 M K_2HPO_4 + 0.1 M KH_2PO_4 (0.1 M PBS) solution, and the main methods include CV and timing amperometry (i-t). Cyclic stability was measured in 0.1 M PBS within the potential range. Sensitivity and detection line analysis were performed by

configuring different concentrations of H_2O_2 solutions at an operating voltage of -0.3 V. Treatment of serum sample: Dilute 20 times with buffer solution to form 5% serum sample, reserve the sample for later use.

1.3 Preparation of electrode

1.3.1 Nickel foam (NF) working electrode

The commercial nickel foam was cut to a size of 1 cm × 3 cm, and then ultrasonicated with HCl, acetone, ethanol, and water for 20 minutes each time, and used as a current collector after being dried in an oven. The active electrode materials HRBNU-7, $Cu_3[P_2W_{18}O_{62}]$, HKUST-1, physical mixture with acetylene black was doped with N-methyl pyrrolidone in a 1:1 ratio to prepare the working electrode. The uniform slurry about 5 mg were coated on the nickel foam collector (1 cm ×1 cm) and dried at room temperature.

1.3.2 The symmetrical double electrode

In a symmetrical double electrode system, a symmetrical supercapacitor (SSC) was assembled with HRBNU-7 as positive and negative electrodes placed on both sides of the isolation plate in a 1 M Na_2SO_4 electrolyte. The weight of the two NF electrodes is roughly the same.

1.3.3 The glass carbon (GCE) working electrode

The GCE (diameter 3 mm) was polished with 1, 0.3, 0.05 mm alumina powder prior to each test and rinsed thoroughly with deionized water after each step. The slurry of the working electrode was prepared by using the mixture of acetylene black and HRBNU-7 hybrid materials in a weight ratio of 1:1 as raw material, ethanol (1 mL) and deionized water (3 mL) as solvents. A well-dispersed slurry (5 μL) was dropped on the GCE surface and dried at room temperature for 2 h to form a uniform film. Then, nafion solution (5 μL, Aldrich) was dropped onto the GCE surface and dried at room temperature.

1.4 Computational formula

The specific capacitance of the three electrodes system is calculated as follow:

$C_s=I\times\Delta t/(m\times\Delta V)$ Equation(S1)

where I (A g^{-1}) is the discharge current and Δt (s) is the discharge time, ΔV (V) is the voltage window, and m (g) is the load of the active material in the electrode.

The formula for calculating the specific capacitance of two electrodes:

$C = 2I \times \Delta t / (m \times \Delta V)$ Equation(S2)

where I is the current density (A g^{-1}), Δt designates the discharge time(s), m signifies mass of both the electrodes (g) and ΔV represents voltage window (V), respectively. The energy density (E, Wh kg^{-1})and power density (P, W kg^{-1}) calculation formulas are as follows:

$E = C\Delta V^2/7.2$ Equation(S3)

$P = E \times 3600/\Delta t$ Equation(S4)

Catalytic efficiency calculation formula:

CAT = 100% × [Ip{compound}H_2O_2 − Ip{compound}] / Ip {compound} Equation(S5)

2. Results and Discussion

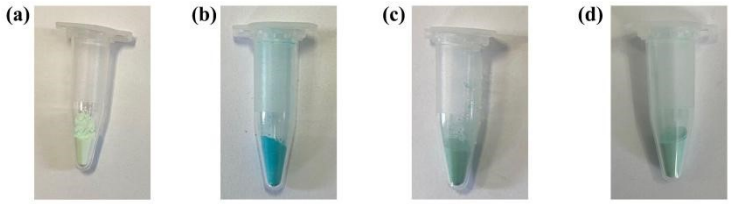

Fig. S1 The colors of (a) $Cu_3[P_2W_{18}O_{62}]$, (b) HKUST-1, (c) HRBNU-7 and (d) physical mixture.

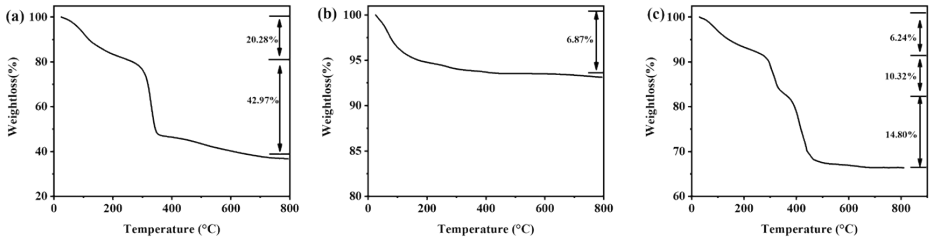

Fig. S2 TG curves of (a) HKUST-1, (b) $Cu_3[P_2W_{18}O_{62}]$ and (c) HRBNU-7.

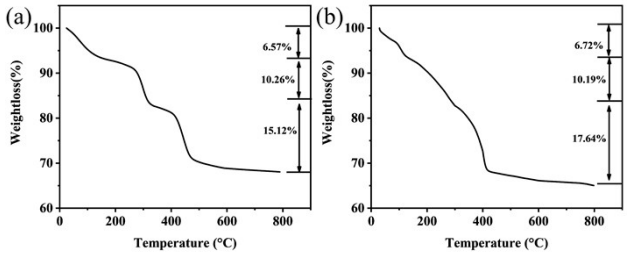

Fig. S3 TG curves of (a) HRBNU-7(-1) and (b) HRBNU-7(-3).

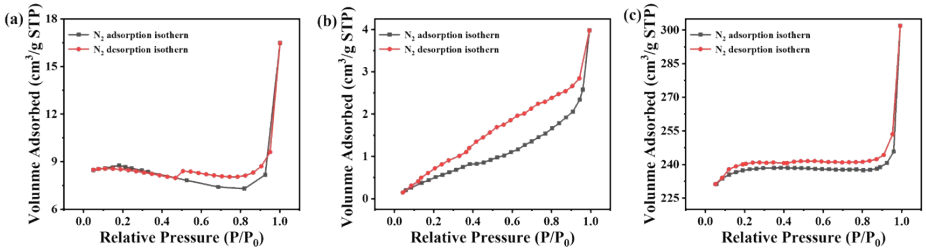

Fig. S4 N_2 adsorption/desorption isotherm of (a) HRBNU-7, (b) $Cu_3[P_2W_{18}O_{62}]$ and (c) HKUST-1.

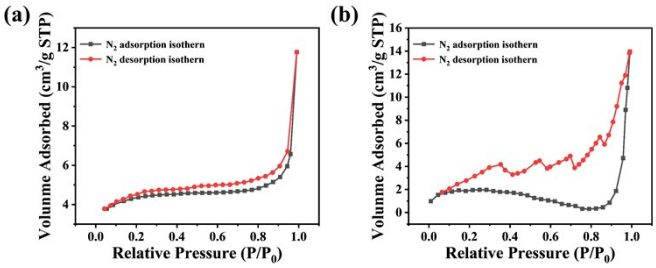

Fig. S5 N_2 adsorption/desorption isotherm of (a) HRBNU-7(-1) and (b) HRBNU-7(-3).

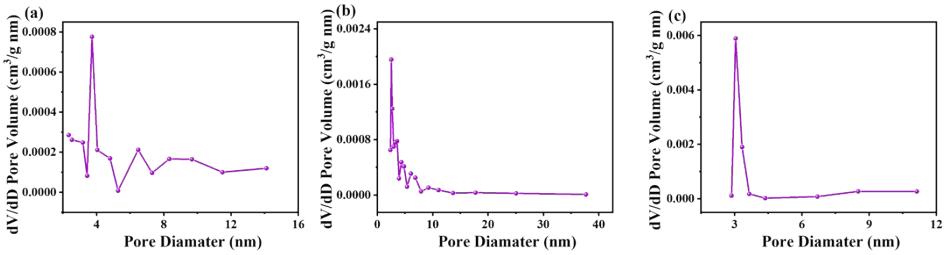

Fig. S6 The pore size distribution of (a) HRBNU-7, (b) $Cu_3[P_2W_{18}O_{62}]$ and (c) HKUST-1.

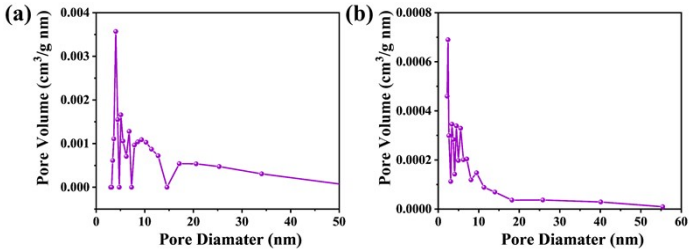

Fig. S7 The pore size distribution of (a) HRBNU-7(-1) and (b) HRBNU-7(-3).

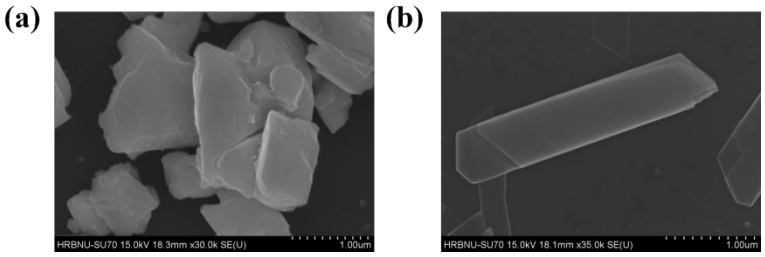

Fig. S8 SEM images of (a) $Cu_3[P_2W_{18}O_{62}]$ and (b) HKUST-1.

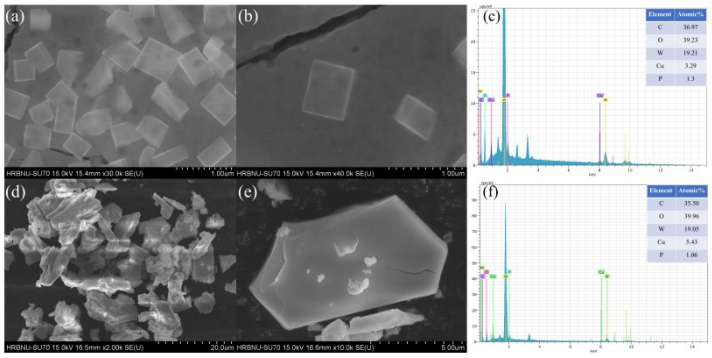

Fig. S9 (a), (b) SEM image and (c) EDS for the HRBNU-7(-1); (d), (e) SEM image and (f) EDS for the HRBNU-7(-3).

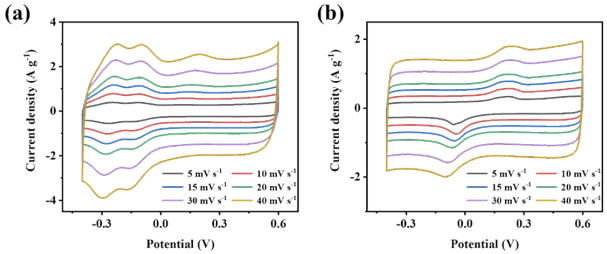

Fig. S10 CV curves of (a) $Cu_3[P_2W_{18}O_{62}]$ and (b) HKUST-1 at different scaning rate with NF as the collector.

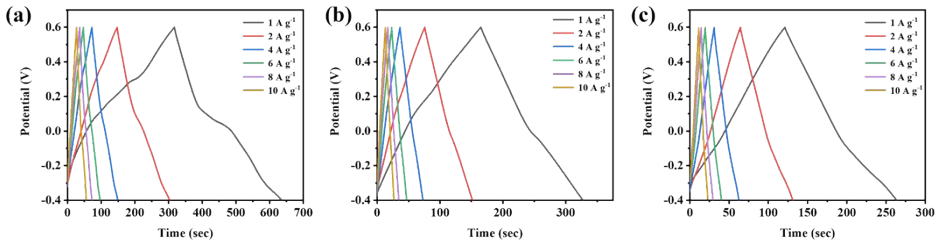

Fig. S11 GCD curves of (a) HRBNU-7, (b) $Cu_3[P_2W_{18}O_{62}]$ and (c) HKUST-1.

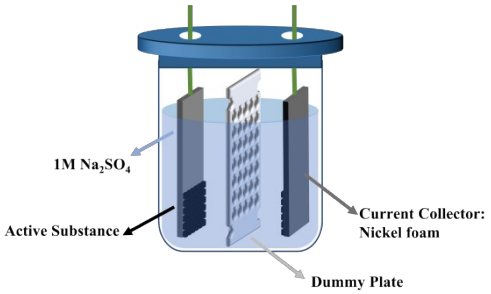

Fig. S12 Schematic diagram of SSC device.

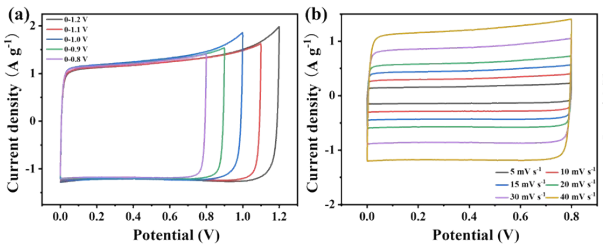

Fig. S13 (a) CV curves under different voltage windows (at the same scan rate), (b) CV curves at different scan rates of 5–40 mV s^{-1} for SSC.

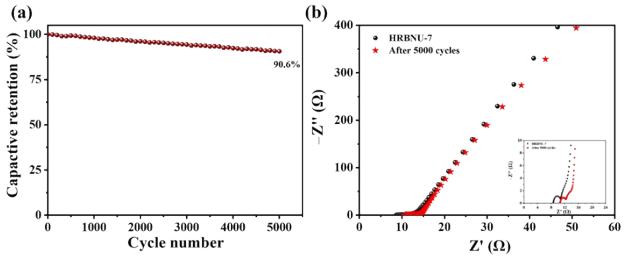

Fig. S14 (a) 5000 cycles and (b) EIS of before and after 5000 cycles of the SSC.

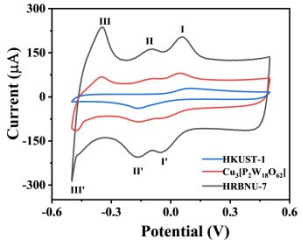

Fig. S15 The CV curves of different compounds at 40 mV s^{-1}.

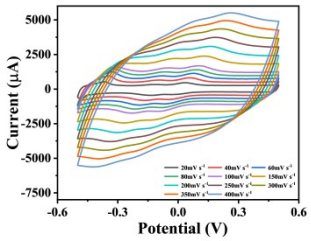

Fig. S16 The CV curves of HRBNU-7 at 20-400 mV s^{-1}.

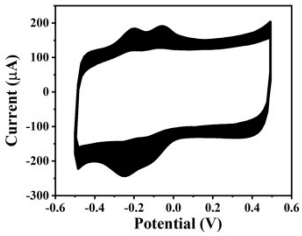

Fig. S17 The CV curves of HRBNU-7 over 1000 cycles.

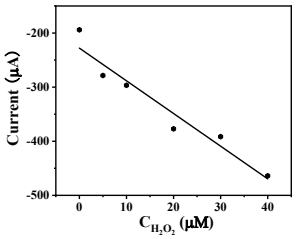

Fig. S18 The plots of the HRBNU-7 cathodic peak currents vs concentrations of H_2O_2.

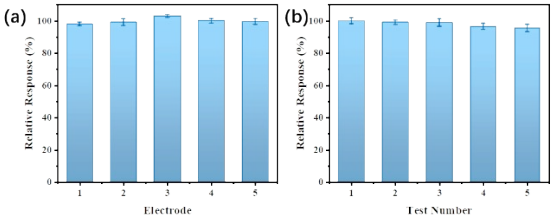

Fig. S19 (a) Reproducibility of five electrodes in the determination of 40 mM H_2O_2, (b) reproducibility experiments with the same electrode.

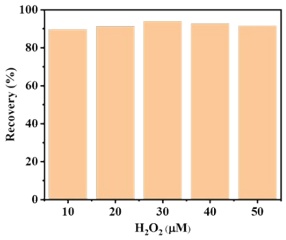

Fig. S20 Recovery values at different concentrations of H_2O_2.

Table S1 IR spectra of different compounds with diffraction peaks

Peaks (cm^{-1}) / Sample	**Benzene ring**		**C-O**	**C=O**	**ν_{as}(P-O_a)**	**ν_{as}(W-O_t)**	**ν_{as}(W-O_b-W)**	**ν_{as}(W-O_c-W)**
HKUST-1	1621.85	1444.97	1375.08	1714.57				
$Cu_3[P_2W_{18}O_{62}]$					1091.22	961.41	912.91	791.67
Physical mixture	1621.85	1444.97	1375.08	1714.57	1091.22	961.41	912.91	791.67
HRBNU-7	1621.85	1444.69	1383.64	1710.29	1092.64	961.41	912.91	793.67
HRBNU-7 (-1)	1621.85	1444.69	1383.64	1710.29	1092.64	961.41	912.91	793.67
HRBNU-7 (-3)	1621.85	1444.69	1383.64	1710.29	1092.64	961.41	912.91	793.67

Table S2 Element contents (wt%) of HRBNU-7 and (-1, -3) characterized by ICP-MS

Samples	P	W	Cu
HRBNU-7(-1)	0.64	43.74	4.76
HRBNU-7	0.74	53.78	7.53
HRBNU-7(-3)	0.55	41.90	6.71

Table S3 The specific capacitance and rate capabilities of various electrodes reported previously POM-based materials

Materials	Specific capacitance	Cycling stability	Current collector	Ref.
$(H_2bpe)(Hbpe)_2\{[Cu(pzta)(H_2O)][P_2W_{18}O_{62}]\}\cdot 5H_2O$	168 F cm^{-2} (5 A g^{-1})	90.7% (1000 cycles)	Glassy carbon	1
Mo_{132}-DTAB-EEG	65 F g^{-1}	99% (5000 cycles)	Carbon cloth	2
AC/$PW_{12}O_{40}$	254 F g^{-1} (10 mV s^{-1})	35% (30000 cycles)	Graphite rods	3
$[\{K(H_2O)\}_2\{Cu_2(biim)_2\}_2(P_2W_{18}O_{62})]$	95.7 F g^{-1} (0.2 A g^{-1})	91.2% (5000 cycles)	Carbon cloth	4
rGO-PMo_{12}	278 mF cm^{-2}	89% (5000 cycles)	Carbon cloth	5
PAni/$H_3PMo_{12}O_{40}$	120 F g^{-1} (0.4 A g^{-1})	70% (1000 cycles)	Rigid graphite plate	6

$AC/PMo_{12}O_{40}$	136 F g^{-1} (2 A g^{-1})	91% (8000cycles)	Glassy carbon	7
$[Cu^{I}H_2(C_{12}H_{12}N_6)(PMo_{12}O_{40})]\cdot[(C_6H_{15}N)(H_2O)_2]$	249 F g^{-1} (3 A g^{-1})	93.5% (1000 cycles)	Glassy carbon	8
$[Cu^{II}_2(C_{12}H_{12}N_6)_4(PMo^{VI}_9Mo^{V}_3O_{39})]$	154.5 F g^{-1} (3 A g^{-1})	91.1% (1000 cycles)	Glassy carbon	8
PPy-PMo_{12}/rGO	252 F g^{-1} (2 A g^{-1})		Au-coated PET	9
$[HPMo^{VI}_9Mo^{V}_3O_{40}]Cu^{I}_5$[4-atrz]$_6\cdot H_2O$	231.7 F g^{-1} (1 A g^{-1})	88.2% (1000 cycles)	Glassy carbon	10
$[HPW^{VI}_9W^{V}_3O_{40}]Cu^{I}_5$[4-atrz]$_6$	147.5 F g^{-1} (1 A g^{-1})	95.3% (1000 cycles)	Glassy carbon	10
$[H_2SiMo^{VI}_9Mo^{V}_3O_{40}]Cu^{I}_5$[4-atrz]$_6\cdot H_2O$	232.5 F g^{-1} (1 A g^{-1})	98.8% (1000 cycles)	Glassy carbon	10
$(Hbipy)_3[PMo_{12}O_{40}]\cdot 3H_2O$	263.9 F g^{-1} (1 A g^{-1})	76.9 % (5000 cycles)	Nickel foam	11
$[Co(bim)_2(H_2O)_2][H_2SiW_{12}O_{40}]\cdot 2H_2O$	186.83 F g^{-1} (1 A g^{-1})	95.1 % (5000 cycles)	Nickel foam	12
$\{Ag_5BW_{12}O_{40}\}$@[Ag_3(μ-Hbtc)(μ-H_2btc)]n	179.1 F g^{-1} (1 A g^{-1})	97.4 % (5000 cycles)	Nickel foam	13
$AC/PMo_{12}O_{40}$	293 F g^{-1} (6 mA cm^{-2})		C250 carbon monoliths	14
$[Ag_5(brtmb)_4][VW_{10}V_2O_{40}]$	206 F g^{-1} (110 A g^{-1})	81.7% (1000 cycles)	Glassy carbon	15
$(NH_4)_{42}[Mo^{VI}_{72}Mo^{V}_{60}O_{372}(CH_3COO)_{30}(H_2O)_{72}]$	617.3 F g^{-1}	66.7% (3000 cycles)	Nickel foam	16
$\{Co_3Mo_7O_{24}\}$@Ag-BTC	260.7 F g^{-1} (1 A g^{-1})	99.8 % (5000 cycles)	Nickel foam	17
Zn-BTC@$Ag_5[BW_{12}O_{40}]$	161.7 F g^{-1} (1 A g^{-1})	92.8 % (5000 cycles)	Nickel foam	18
$[\{Na(H_2O)(H_2btb)\}\{Cu^{I}_4(H_2O)(pz)_5Cl\}\{H_2Sr\subset P_6Mo_2{}^{V}Mo_{16}{}^{VI}O_{73}\}]\cdot 3H_2O$	929.4 F g^{-1} (3 A g^{-1})	94.1 % (5000 cycles)	Graphene oxide composite carbon paper electrode	19

$(H_4btb)[H_4Sr\subset P_6Mo_2^{V}Mo_{16}^{VI}O_{73}]\cdot 3H_2O$	599.1 F g^{-1} (3 A g^{-1})	90.4 % (5000 cycles)	Graphene oxide composite carbon paper electrode	19
$[Cu^{I}_4H_2(btx)_5(PW_{12}O_{40})_2]\cdot 2H_2O$	100 F g^{-1} (2 A g^{-1})	90% (1000 cycles)	Glassy carbon	20
$[Cu^{II}Cu^{I}_3(H_2O)_2(btx)_5(PW^{VI}_{10}W^{V}_2O_{40})]\cdot 2H_2O$	82.1 F g^{-1} (2 A g^{-1})	100% (1000 cycles)	Glassy carbon	20
$[Cu^{I}_6(btx)_6(PW^{VI}_9W^{V}_3O_{40})]\cdot 2H_2O$	76.4 F g^{-1} (2 A g^{-1})	100% (1000 cycles)	Glassy carbon	20
$[Cu^{II}Cu^{I}_3(btx)_5(SiMo^{VI}_{11}Mo^{V}O_{40})]\cdot 4H_2O$	138.4 F g^{-1} (2 A g^{-1})	97% (1000 cycles)	Glassy carbon	20
$[Cu^{I}_4H_2(btx)_5(PMo_{12}O_{40})]\cdot 2H_2O$	237 F g^{-1} (2 A g^{-1})	92.5% (1000 cycles)	Glassy carbon	20
$[H_5(SiW_9^{VI}W_3^{V}O_{40})_3Ni_8(H_2O)_{12}(atrz)_{12}]\cdot 12H_2O(SiW_{12}\text{-}Ni_8)$	150.8 F g^{-1} (1 A g^{-1})	76.84% (1000 cycles)	Glassy carbon	21
$[H_2(PW_9^{VI}W_3^{V}O_{40})_3Ni_8(H_2O)_{12}(atrz)_{12}]_{1/3}\cdot 4H_2O$	236.3 F g^{-1} (1 A g^{-1})	83.33% (1000 cycles)	Glassy carbon	21
$[H_{11}(CoW_9^{VI}W_3^{V}O_{40})_3Ni_8(H_2O)_{12}(atrz)_{12}]\cdot 12H_2O$	526.6 F g^{-1} (1 A g^{-1})	93.76% (1000 cycles)	Glassy carbon	21
$[H_{11}(CoW_9^{VI}W_3^{V}O_{40})_3Co_8(H_2O)_{12}(atrz)_{12}]\cdot 12H_2O$	509.4 F g^{-1} (1 A g^{-1})	85.94% (1000 cycles)	Glassy carbon	21
$H_3[Cu_2(4\text{-}dpye)_2(PMo_{12}O_{40})]$	260.0 F g^{-1} (0.5 A g^{-1})	94.6% (2000 cycles)	Carbon cloth	22
$L_{0.5}[Cu_2L_{3.5}(SiW_{12}O_{40})]$	159.2 F g^{-1} (3 A g^{-1})		Glassy carbon	23
PW_{12}@MIL-101/PPy-0.15	1124 mF cm^{-2} (0.5 mA cm^{-2})		Nickel foam	24
PW_{12}@MIL-101	158 mF cm^{-2} (0.5 mA cm^{-2})		Nickel foam	24
$[H(C_{10}H_{10}N_2)Cu_2][PMo_{12}O_{40}]$	287 F g^{-1} (1 A g^{-1})	81.5% (500 cycles)	Glassy carbon	25
$[H(C_{10}H_{10}N_2)Cu_2][PW_{12}O_{40}]$	153.43 F g^{-1} (1 A g^{-1})	18.2% (500 cycles)	Glassy carbon	25
$H_3PMo^{VI}_{12}O_{40}\cdot(BPE)_{2.5}\cdot 3H_2O$	137.5 F g^{-1} (2 A g^{-1})	92% (1000 cycles)	Glassy carbon	26
$[Cu^{I}(btx)]_4[SiW_{12}O_{40}]$	110.3 F g^{-1} (3 A g^{-1})	87% (1000 cycles)	Glassy carbon	27

$[\{Cu^{II}_6(btx)_7(H_2O)_{12}\}H_4(W_{12}O_{40})_2]\cdot 12H_2O$	50.0 F g^{-1} (3 A g^{-1})	87.5% (1000 cycles)	Glassy carbon	27
HRBNU-7	318.6 F g^{-1} (1 A g^{-1})	92.36% (5000 cycles)	Nickel foam	This work

Table S4 Comparison of electrocatalytic performances of the H_2O_2 sensor with other recently reported electrodes modified.

Electrode	**Linear range (mM)**	**Sensitivity (μA mM^{-1} cm^{-2})**	**Detection limit (μM)**	**Reference**
CdO/MWCNT /GCE	0.0005-0.20	-	0.10	28
P_2W_{18}/CNTs/AuNPs	0.001-0.098	596.1	0.052	29
PEI/rGO}-Au@P_8W_{48}	0-137.15	40.84	0.31	30
ERGO/Au NPs/POM	-	381.5	0.56	31
CePW/MWNTs	0.00025-0.0115	-	0.03	32
Co_3O_4/rGO/GCE	0.015-0.675	1140	2.40	33
Fe_2O_3/rGO/GCE	0.05-9.00	-	6.00	34
MnO_2/rGO/CNT/GCE	0.001-1.03	-	0.10	35
α-MoO_3/GO/GCE	0.00092-2.46	391.39	0.31	36
Fe_3O_4/NMCMs /GCE	0.05-33.08	77.1	5.89	37
CdO/MWCNT /GCE	0.0005-0.20	-	0.10	38
NENU5-KB-3/GCE	0.01-20	33.77	1.03	39
Cu-AlW_{12}/AC/GCE	0.0195-0.9	-	0.86	40
POMOF-2/AC/GCE	0.00143-1.89	484.02	0.48	41
SWCNT-CO-$(APy)_6[H_2W_{12}O_{40}]$	0.1-0.8	2289.3	0.4	42
$Ni(OH)_2$-PMA SHNWs	5-50	-	0.05	43
MIL-101(Fe)@P_2W_{18}@ SWNT	0-0.08	-	0.3	44
Mn_3O_4-CeO_2/GCE	0.005-17	176.4	0.00381	45
HRBNU-7	0.0005-0.3	2113.5	0.17	This work

References

[1] G. N. Wang, T. T. Chen, S. B. Li, H. J. Pang, H. Y. Ma, *Dalton Trans*., 2017, **46**, 13897-13902.

[2] D. Pakulski, A. Gorczyński, W. Czepa, Z. Y. Liu, L. Ortolani, V. Morandi, V. Patroniak, A. Ciesielski, P. Samorì, *Energy Stor. Mater.*, 2019, **17**, 186-193.

[3] J. Suárez-Guevara, V. Ruiz, P. Gomez-Romero, *J. Mater. Chem.,* 2014, **2**, 1014-1021.

[4] J. Q. Gao, L. G. Gong, X. Y. Fan, K. Yu, Z. W. Zheng, B. B. Zhou, *ACS Appl. Nano Mater*., 2020, **3**,1497-1507.

[5] D. P. Dubal, N. R. Chodankar, A. Vinu, D. H. Kim, P. Gomez-Romero, *ChemSusChem*, 2017, **10**, 2742-2750.

[6] A. K. Cuentas-Gallego, M. Lira-Cantú, N. Casañ-Pastor, P. Gomez-Romero, *Adv. Funct. Mater.*, 2005, **15**, 1125-1133.

[7] V. Ruiz, J. Suárez-Guevara, P. Gomez-Romero, *Electrochem. Commun.*, 2012, **24**, 35-38.

[8] D. F. Chai, J. J. Xin, B. N. Li, H. J. Pang, H. Y. Ma, K. Q. Li, B. X. Xiao, X. M. Wang, L. C. Tan, *Dalton Trans.*, 2019, **48**, 13026-13033.

[9] Y. Y. Chen, M. Han, Y. J. Tang, J. C. Bao, S. L. Li, Y. Q. Lan, Z. H. Dai, *Chem. Commun.*, 2015, **51**, 12377-12380.

[10] M. L. Yang, S. Rong, X. M. Wang, H. Y. Ma, H. J. Pang, L. C. Tan, Y. X. Jiang, K. Q. Gao, *ChemNanoMat*, 2021, **7**, 299-306.

[11] L. Y. Zhang, X. Y. Zhao, C. M. Wang, K. Yu, J. H. Lv, C. X. Wang, B. B. Zhou, *J. Solid State Chem.*, 2022, **312**, 123235.

[12] Y. Liang, H. Liu, L. G. Gong, C. X. Wang, C. M. Wang, K. Yu, B. B. Zhou, *Chem. J. Chinese Universities*, 2022, **43**, 20210556.

[13] Y. Liang, N. Kang, C. M. Wang, K. Yu, J. H. Lv, C. X. Wang, B. B. Zhou, *Dalton Trans*., 2022, **51**, 7613-7621.

[14] P. Palomino, J. Suarez-Guevara, M. Olivares-Marín , V. Ruiz, D. P. Dubal, P. Gómez-Romero, *D. Tonti, E. Enciso*, 2017, **111**, 74-82.

[15] G. N. Wang, T. T. Chen, X. M. Wang, H. Y. Ma, H. J. Pang, *Eur. J. Inorg. Chem.*, 2017, **45**, 5350-5355.

[16] Y. N. Dong, L. Chen, W. L. Chen, X. T. Zheng, X. L. Wang, E. B. Wang, *Chem. Asian J.*, 2018, **13**, 3304-3313.

[17] L. J. Xu, X. Y. Zhao, K. Yu, C. M. Wang, J. H. Lv, C. X. Wang, B. B. Zhou, *CrystEngComm*, 2022, **24**, 5614-5621.

[18] L. Y. Wang, N. Kang, L. G. Gong, C. X. Wang, K. Yu, C. M. Wang, B. B. Zhou, *J. Energy Storage*, 2022, **46**, 103873.

[19] T. T. Zhao, L. P. Cui, K. Yu, J. H. Lv, Y. J. Ma, A. S. Yang, B. B. Zhou, *ACS Appl. Mater. Interfaces*, 2022, **14**, 30099-30111.

[20] D. F. Chai, C. J. Gómez-García, B. N. Li, H. J. Pang, H. Y. Ma, X. M. Wang, L. C. Tan, *Chem. Eng. J.*, 2019, **373**, 587-597.

[21] Y. Q. Zhao, M. L. Yang, S. Rong, X. M. Wang, H. Y. Ma, H. J. Pang, L. C. Tan, K. Q. Gao, *J. Electroanal. Chem*., 2021, **882**, 115017.

[22] Q. Q. Liu, X. L. Wang, H. Y. Lin, Z. H. Chang, Y. C. Zhang, Y. Tian, J. J. Lu, L. Yu, *Dalton Trans.*, 2021, **50**, 9450-9456.

[23] J. X. Wang, L. Zhang, L. J. Zhao, T. Li, S. B. Li, *J. Mol. Struct.*, 2021, **1231**, 129966.
[24] T. Y. Li, P. He, Y. N. Dong, W. C. Chen, T. Wang, J. Gong, W. L. Chen, *Eur. J. Inorg. Chem.*, 2021, **2021**, 2063-2069.
[25] S. Roy, V. Vemuri, S. Maiti, K. S. Manoj, U. Subbarao, S. C. Peter, *Inorg. Chem.*, 2018, **57**, 12078-12092.
[26] C. L. Wang, S. Rong, Y. Q. Zhao, X. M. Wang, H. Y. Ma, *Transit. Met. Chem.*, 2021, **46**, 335-343.
[27] D. F. Chai, Y. Hou, K. P. O'Halloran, H. J. Pang, H. Y. Ma, G. N. Wang, X. N. Wang, *ChemElectroChem*, 2018, **5**, 3443-3450.
[28] N. Butwong, L. Zhou, W. Ng-eontae, R. Burakham, E. Moore, S. Srijaranai, J. H. Luong, J. D. Glennon, *Journal of Electroanalytical Chemistry*, 2014, **717-718**, 41-46.
[29] S. Guo, L. Xu, B. Xu, Z. Sun, L. Wang, *Analyst*, 2015, **140**, 820–826.
[30] X. Zhang, Y. Bao, Y. Bai, Z. Chen, J. Li and F. Feng, *Electrochim. Acta*, 2019, **300**, 380–388.
[31] S. Berbec´, S. Z˙ola˛dek, A. Jabłon´ska and B. Pałys, *Sens. Actuators*, 2018, **258**, 745–756.
[32] B. Fang, D. Chen, Q. Huang, Y . Wei, G. Wang, *Electroanalysis*, 2008, **20**, 1234.
[33] L. J. Kong, Z. Y. Ren, N. N. Zheng, S. C. Du, J. Wu, J. L. Tang, H. G. Fu, *Nano Res*, 2015, **8**, 469.
[34] M. A. Karimi, F. Banifatemeh, A. Hatefifi-Mehrjardi, H. Tavallali, Z. Eshaghia, G. Deilamy-Rad, *Mater. Res. Bull*, 2015, **70**, 856.
[35] D. X. Ye, H. X. Li, G. H. Liang, J. Luo, X. X. Zhang, S. Zhang, H. Chen, J. L. Kong, *Electrochim. Acta*, 2013, **109**, 195.
[36] B. Li, H. Y. Song, Z. P. Deng, L. H. Huo, S. Gao, *Sensors & Actuators: B. Chemical*, 2019, **288**, 641.
[37] Z. J. Qin, Y. Zhao, L. Lin, P. Zou, L. Zhang, H. Chen, Y. Wang, G. T. Wang, Y. S. Zhang, *Microchim Acta*, 2017, **184**, 4513.
[38] N. Butwong, L. Zhou, W. Ng-eontae, R. Burakham, E. Moore, S. Srijaranai, J. H. T. Luong, J. D. Glennon, *J. Electroanal. Chem*, 2017, **717**, 41.
[39] C. Wang, M. Zhou, Y. Y. Ma, H. Q. Tan, Y. H. Wang, Y. G. Li, *Chemistry: An Asian Journal*, 2018, **13**, 2054.
[40] L. G. Gong, X. X. Qia, K. Yu, J. Q. Gao, B. B. Zhou, G. Y. Yang, *J. Mater. Chem. A.*, 2020, **8**, 5709.
[41] L.P. Cui, K. Yu, J.H. Lv, C.H. Guo, B.B. Zhou, *J. Mater. Chem. A.*, 2020, **8**, 22918.
[42] Y. Sahraoui, S. Chaliaa, A. Maaref, A. Haddad, F. Bessueille, Ni. Jaffrezic-Renault, *Electroanalysis*, 2020, **32**, 683-689.
[43] J. L. Liu, J. Zhuang, W. X. Shi, X. Wang, *Chem. Mater.*, 2021, **33**, 7100−7105.
[44] X. Y. Liu, Q. Y. Zheng, D. Q. Jia, W. W. Wang, H. Zhao, X. S. Tao, J. Q. Sha, *Journal of Cluster Science*, 2023, Accepted.
[45] L. Liu, X. X. Yan, Y. R. Zhang, D. M. Deng, H. B. He, Y. Y. Lei, X. Shen, L. Q. Luo, *ACS Appl. Nano Mater.,* 2023, **6**, 2116−2124.